Acta Crystallographica Section B
Structural Science
ISSN 0108-7681

Structures of tetrabromothiophene and tetrabromoselenophene: the influence of the heteroatom on the heterophene packing

Robert B. Helmholdt,[a]* Ed J. Sonneveld,[b] Christophe M. L. Vande Velde,[b] Frank Blockhuys,[b] Albert T. H. Lenstra,[b] Herman J. Geise[b] and René Peschar[a]

[a]Laboratory for Crystallography, Van't Hoff Institute for Molecular Sciences (HIMS), Faculty of Science (FNWI), University of Amsterdam, Valckenierstraat 65, NL-1018 XE Amsterdam, The Netherlands, and [b]University of Antwerpen (UIA), Department of Chemistry, Universiteitsplein 1, B-2160 Wilrijk, Belgium

Correspondence e-mail: rbh@science.uva.nl

Received 2 May 2007
Accepted 25 July 2007

Dedicated to the memory of Professor Herman Geise – our teacher and friend.

The crystal structures of C_4Br_4S and C_4Br_4Se have been determined from X-ray powder diffraction data, using direct-space search techniques. In the case of C_4Br_4S two crystalline phases occur, a stable orthorhombic and a metastable monoclinic phase. For the orthorhombic phase two different structural models were found that fit the experimental data equally well. The diversity in crystal structure models and packings of C_4Br_4S is explained.

1. Introduction

Tetrabromothiophene (C_4Br_4S) and its selenophene analogue tetrabromoselenophene (C_4Br_4Se) are two rare examples of organic molecules of which the usual outside lining of small, hard H atoms has been replaced by one of large, soft π-electron-rich Br atoms. With respect to C_4Br_4S, the possible influence of the thus screened π-electron system on the physico-chemical properties has attracted considerable attention and the list of its material characteristics investigated to date is impressive (see Blockhuys *et al.*, 2000, and references therein). In this latter paper a vibrational analysis of C_4Br_4S was presented in which a number of bands in the Raman spectrum was assigned as line splittings owing to crystal effects. These splittings helped to assign the correct space group based on laboratory X-ray powder diffraction data. Although the crystal structure of C_4Br_4S had not been refined completely at the time of that work, it had already become obvious that the packing is dominated by the Br atoms striving for a close-packed arrangement that is frustrated by the remainder of the molecule, *i.e.* the C_4S fragment, and its particular geometry. A number of other solid-state properties could be rationalized from this packing that is characterized by a dense bromine matrix in which thiophene rings are dispersed with restricted long-range order. This raised the question whether C_4Br_4S is unique in this respect. Since the natural geometric construction of the thiophene ring in C_4Br_4S distorts the close-packed arrangement of the Br atoms, other tetrabromoaromatics, of which the size of the ring is different, may influence the bromine packing, and thus the resulting chemical behaviour, in a completely different way. In view of this, it was attempted to synthesize other 2,3,4,5-tetrabromoaromatics, but only C_4Br_4Se yielded (poly)-crystalline material suitable for X-ray diffraction analysis.

In this paper we present the full experimental details and the definitive molecular and crystal structures of C_4Br_4S and C_4Br_4Se, as determined from X-ray powder diffraction data and direct-space search techniques. In the case of C_4Br_4S an orthorhombic and a monoclinic crystalline phase have been identified; for the orthorhombic one two different structural models can be fitted to the experimental data equally well. On

Table 1
Experimental data and unit-cell parameters (based on Guinier data and Rietveld Refinement) of α-C_4Br_4S, β-C_4Br_4S and C_4Br_4Se.

Compound	α-C_4Br_4S	β-C_4Br_4S		C_4Br_4Se
Guinier data (T = 295 K)				
a (Å)	12.672 (3)	12.417 (2)		14.928 (2)
b (Å)	4.043 (1)	4.0386 (4)		4.122 (1)
c (Å)	16.378 (5)	8.825 (1)		13.991 (2)
β (°)		109.20 (1)		96.37 (1)
V (Å^3)	839.1 (4)	417.9 (1)		855.6 (2)
Space group	$Pca2_1$	Pn		$P2_1/c$
M_{20}†	34	36		36
Rietveld Refinement				
	Synchrotron	Guinier	Synchrotron	Synchrotron
T (K)	200	295	200	200
a (Å)	12.6511 (8)	12.419 (5)	12.393 (5)	14.86453 (4)
b (Å)	4.0371 (3)	4.040 (2)	3.996 (2)	4.07898 (2)
c (Å)	16.3449 (11)	8.824 (4)	8.778 (4)	13.90429 (7)
β (°)	–	109.18 (1)	109.63 (1)	96.350 (1)
V (Å^3)	834.8 (2)	418.1 (5)	409.5 (5)	837.874 (4)
M_r	399.7	399.7	399.7	446.6
D_x (Mg m^{-3})	3.18	3.24	3.22	3.54
μ (mm^{-1})	13.26	13.53	13.47	14.61

† For the definition of the figure-of-merit M_{20} see de Wolff (1968)

Table 2
Results of the full pattern decomposition (FPD) and the model determination.

Compound	α-C_4Br_4S Synchrotron	β-C_4Br_4S Guinier	C_4Br_4Se Synchrotron
Wavelength (Å)	1.25011	1.54056	1.25007
FPD			
2θ range (°)	7.5–82.0		5.0–60.0
R_p	0.078		0.080
R_{wp}	0.104		0.115
S	2.6		3.8
Model determination	Grid search	*FOX*	Grid search
$R(F^2)/R_{wp}$	0.366	0.271	0.220

the basis of the structural models of these phases and an analysis of their packing, it is explained why for C_4Br_4S different models and crystalline packings occur, while C_4Br_4Se does not show this effect.

2. Materials and methods

2.1. Synthesis and crystallization

2.1.1. Tetrabromothiophene, C_4Br_4S. Tetrabromothiophene was synthesized as previously reported (Blockhuys *et al.*, 2000). Attempts to solve the crystal structure from single crystals failed due to the large mosaic spread of up to 20°. Depending on the precise conditions, C_4Br_4S turned out to crystallize in two polycrystalline phases, referred to as α-C_4Br_4S and β-C_4Br_4S. The solid material obtained after recrystallization and subsequent sublimation (batch 1) consisted only of the stable orthorhombic α-phase. However, batch 2, obtained *via* recrystallization from solution, contained a mixture of the α-phase and a monoclinic β-phase. In a closed container, over a period of 5 years, the amount of β-phase slowly decreased in favour of the α-phase, presumably through sublimation of the β-phase and subsequent recondensation as the α-phase.

2.1.2. Tetrabromoselenophene, C_4Br_4Se. Selenophene (2.5 g, 0.019 mol) was dissolved in $CHCl_3$ (10 ml). This solution was cooled to 273 K in an ice bath and subsequently excess bromine (13.0 g, 0.130 mol) was added dropwise over the course of 2 h. The solution was refluxed overnight. A 2*M* solution of KOH in water (50 ml) was added after cooling, and after vigorous stirring the resulting precipitate was filtered. The organic phase was isolated, the solvent was removed and the resulting mixture was chromatographed on silica with a CH_2Cl_2/hexane (30/70) elute. The first band off the column is tetrabromoselenophene. After removing the solvent a creamy white powder was obtained; m.p. 370–371 K. The yield is 3.4 g (39%). $\delta^{13}C$ ($CDCl_3$, 100 MHz, TMS): 112.22 (C2 and C5), 117.98 (C3 and C4). APCI-MS: m/z 439, 442, 444, 446, 448, 450, 451, 452, 453; this is consistent with C_4Br_4Se.

2.2. Methods

2.2.1. Sample preparation, data collection and indexing. The samples were powdered carefully and were then sprinkled onto a Guinier–Johannson sample holder (using a small amount of grease) in order to prevent texture. The sample holder was rotated in the specimen plane during exposure to improve the particle statistics. Several Guinier–Johannson photographs have been taken to allow the recording of very weak as well as very strong reflections.

Using a Johannson LS18 microdensitometer the Guinier films were digitized from 4.00 to 83.00° 2θ in steps of 0.01° 2θ. The lines obtained in this manner were indexed using the cell-indexing program *ITO* (Visser, 1969) and refined using the program *LSPAID* (Visser, 1986). Experimental data, including cell parameters after indexing and after Rietveld refinement of α-C_4Br_4S, β-C_4Br_4S and C_4Br_4Se, are listed in Table 1.[1] Note that in the case of α-C_4Br_4S the space group $Pca2_1$ (29) was chosen instead of the centrosymmetric space group *Pbcm* (57) on the basis of an analysis of the Raman spectrum (Blockhuys *et al.*, 2000).

Synchrotron data collection was carried out at the high-resolution powder diffraction station ID31 (Fitch, 1996, 2004) at the ESRF (Grenoble, France) at a wavelength of 1.25 Å. The capillaries (diameter 0.3 mm) were rotated during exposure. To minimize radiation damage the samples were cooled at 200 K. Continuous scans were recorded at 5° 2θ min^{-1}. The higher-angle regions of the patterns were measured several times in order to mimic a single-crystal measurement as much as possible, *i.e.* to expose each reflection to the same amount

[1] Supplementary data for this paper are available from the IUCr electronic archives (Reference: AV5088). Services for accessing these data are described at the back of the journal.

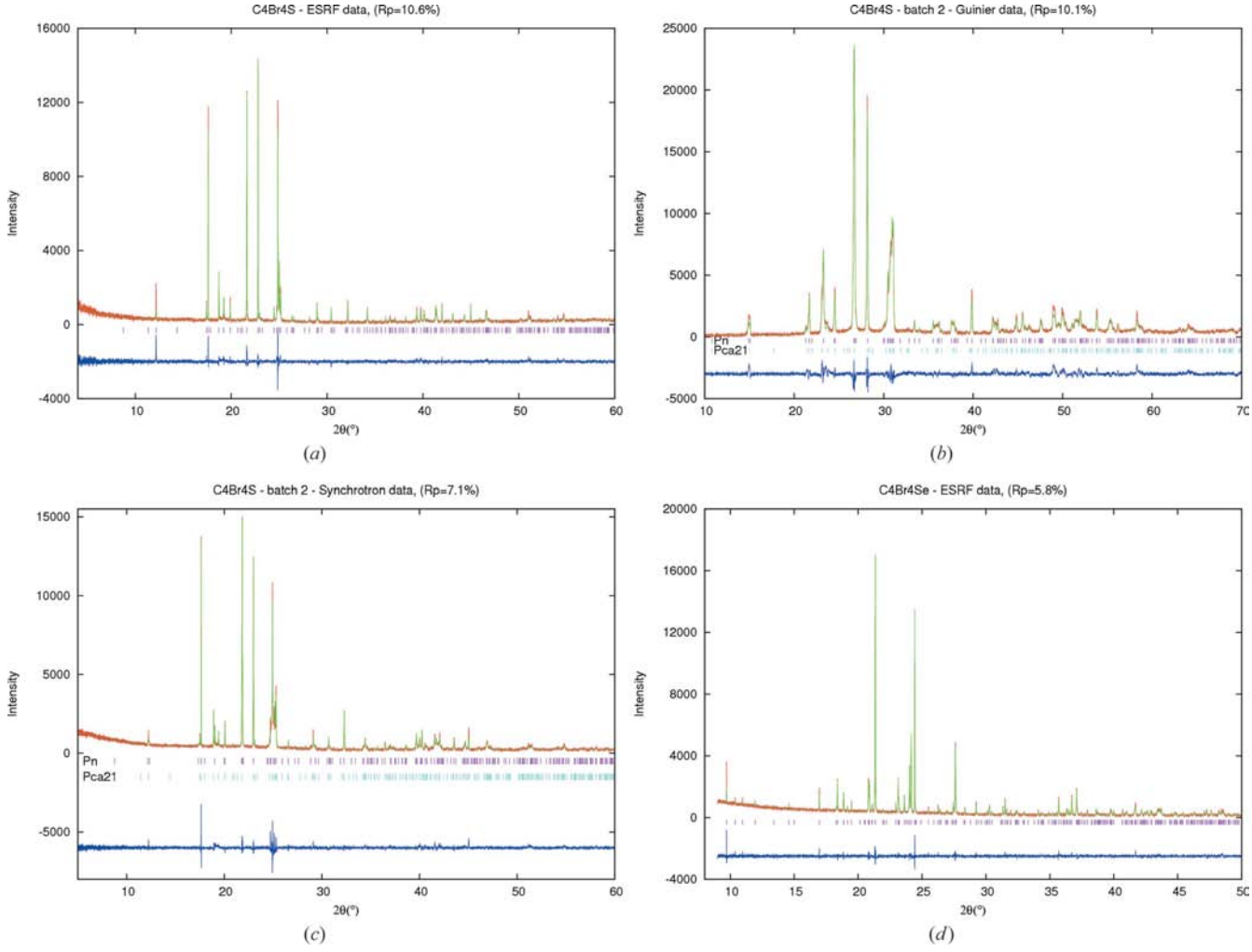

Figure 1
(*a*) Synchrotron powder diffraction pattern of α-C_4Br_4S (batch 1), observed pattern (red), calculated pattern of model A (green) and difference pattern (observed − calculated); (*b*) Guinier powder diffraction pattern of batch 2, both β-C_4Br_4S (monoclinic, main component) and α-C_4Br_4S (orthorhombic) refined; (*c*) synchrotron powder diffraction pattern of batch 2, both α-C_4Br_4S (orthorhombic, main component) and β-C_4Br_4S (monoclinic) refined; (*d*) synchrotron powder diffraction pattern of C_4Br_4Se [as in (*a*)]. A colour version of this figure is available in the online edition of the journal.

of X-rays. After data collection the scans were binned at 0.005° 2θ and scaled.

The synchrotron intensities have been corrected for absorption using the program ABSCYL (R. Lelieveld and R. B. Helmholdt, unpublished) and the digitized Guinier intensities using the method of Sas & de Wolff (1966), assuming an apparent density of 50%. The observed patterns are given in Fig. 1.

2.2.2. Crystal structure determination from Guinier data. In the case of α-C_4Br_4S and C_4Br_4Se the full-pattern decomposition (FPD) procedure in the program *MRIA* (Zlokazov & Chernyshev, 1992) was used to obtain reflection intensities. The powder diffraction patterns were fitted employing a split-type pseudo-Voigt peak profile function (Toraya, 1986). The results of the FPD procedure are summarized in Table 2.

Idealized C_4Br_4S and C_4Br_4Se molecules were used as search models. The molecules were positioned in the asymmetric part of the unit cell with an in-house modified genetic algorithm version of the grid-search procedure (Chernyshev & Schenk, 1998) that is implemented in the program *MRIA* (Zlokazov & Chernyshev, 1992), using a small number of low-angle X_{obs} values extracted from the patterns after the FPD procedure. $R(X)$ values are listed in Table 2 [X_{obs} and $R(X)$ are defined in expressions (1) and (2) of Chernyshev & Schenk, 1998].

The crystal structure of β-C_4Br_4S has been solved using the program *FOX* (Favre-Nicolin & Černý, 2002).

2.2.3. Refinement. The solutions found with the structure determination programs were used as starting models in the Rietveld refinement module of the program *GSAS* (Larson & Von Dreele, 2004), using soft constraints for bond distances, angles and the molecular plane. Synchrotron data were used in the Rietveld refinement, except where stated otherwise. A shifted Chebyschev polynomial was used as the background function. To describe the peak shape the convolution of a pseudo-Voigt with an asymmetry function which uses a semi-empirical microstrain broadening description (Stephens, 1999) was used for the synchrotron data. For the Guinier data an

Table 3
Results of the Rietveld refinements for the X-ray data.

Compound	α-C_4Br_4S Synchrotron			β-C_4Br_4S Guinier	β-C_4Br_4S Synchrotron	C_4Br_4Se Synchrotron
T (K)	200			295	200	200
2θ range (°) measured	4.0–78.0			4.0–80.0	2.0–68.0	9.0–68.0
2θ range(°) refined	4.0–60.0			10.0–70.0	5.0–60.0	9.0–50.0
% β-C_4Br_4S				57.5 (6)	47.7 (7)	
% α-C_4Br_4S				42.5	52.3	
Model	A	B	AB			
% model A	100	–	86.1 (4)			
% model B	–	100	13.9 (4)			
R_p	0.106	0.108	0.104	0.101	0.071	0.058
R_{wp}	0.140	0.142	0.137	0.134	0.096	0.080
$R(F^2)$	0.192	0.191	0.157	0.202	0.165	0.108
GOF	2.5	2.5	2.4	3.8	2.1	1.6

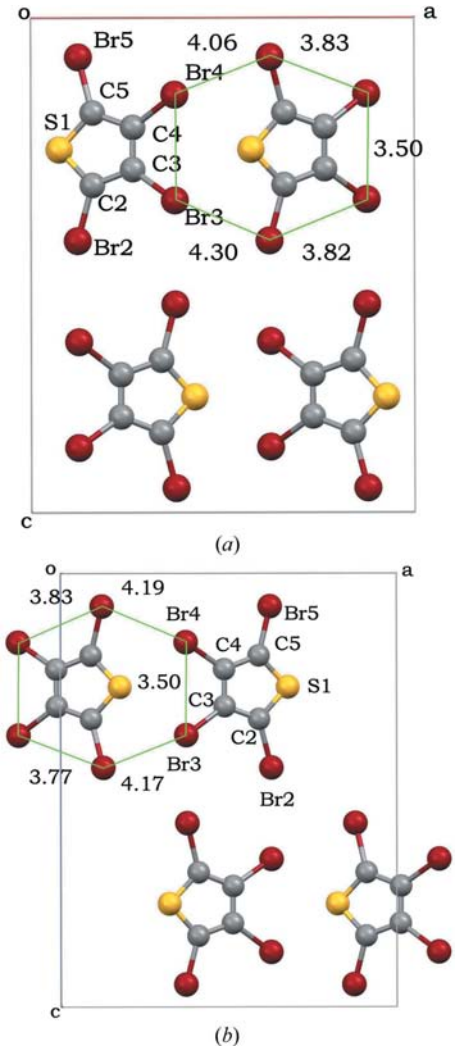

Figure 2
(*a*) Projection of α-C_4Br_4S onto the *ac* plane for model A. (*b*) projection of α-C_4Br_4S onto the *ac* plane for model B using the program *MERCURY* (Macrae *et al.*, 2006). Br—Br distances in Å.

empirical extension of the microstrain anisotropy was used. The final coordinates and isotropic atomic displacement parameters of the structures have been deposited.

3. Results and discussion

3.1. α-C_4Br_4S

During the refinement of α-C_4Br_4S it became clear that two different structural models could be fitted almost equally well to the experimental data. The sole difference between these models, referred to as *A* and *B* (Figs. 2*a* and *b*, respectively), is the orientation of the molecules with respect to the symmetry elements in the unit cell. The calculated powder diffraction patterns of models A and B are nearly identical and their difference trace (A − B) shows no significant differences (Fig. 3). This phenomenon can be explained by the small scattering power of C (and S) compared with that of Br (the scattering power of C *versus* Br is the same as for H *versus* C), and by the fact that the *intra*molecular Br···Br distance is nearly equal to the shortest *inter*molecular Br···Br distance (Figs. 2*a* and *b*). Consequently, the crystal structure models are heavily dominated by the Br-atom framework, which is demonstrated in Figs. 4(*a*) and (*b*), where the overlap of the Br atoms for both models is shown. The refinement of the individual models A and B did not result in a clear preference for either one of them (see Table 3). The refinement of a combined model AB (= A + B), however, with the occupation of the molecules *A* and *B* as an extra parameter led to a slight preference for the presence of model A [86.1 (4)% *A* and 13.9 (4)% *B*]. The observed, calculated and difference patterns for model A are given in Fig. 1(*a*). In an attempt to obtain an unambiguous solution, TOF neutron data have been collected at the HRPD at ISIS, but a refinement against these data also did not result in a clear preference for either model (Table 4).

3.2. β-C_4Br_4S

The Rietveld refinement of β-C_4Br_4S has been carried out with digitized Guinier data and synchrotron data (Table 3). From the Guinier data, which were recorded immediately after the preparation of batch 2, it was concluded that the main constituent has a monoclinic cell, while the synchrotron data of the same sample 5 years later led to an orthorhombic main constituent that was established to be α-C_4Br_4S, implying that the monoclinic phase is not stable. After solving the crystal structures of both α-C_4Br_4S and β-C_4Br_4S, it was established that the amount of β-C_4Br_4S in batch 2 had changed from 57.5 (6) to 47.7 (7)% over the course of 5 years. The observed, calculated and difference patterns of the Guinier and the synchrotron data are given in Figs. 1(*b*) and (*c*), respectively. The structure of β-C_4Br_4S is given in Fig. 5. The results of the refinements are listed in Table 3.

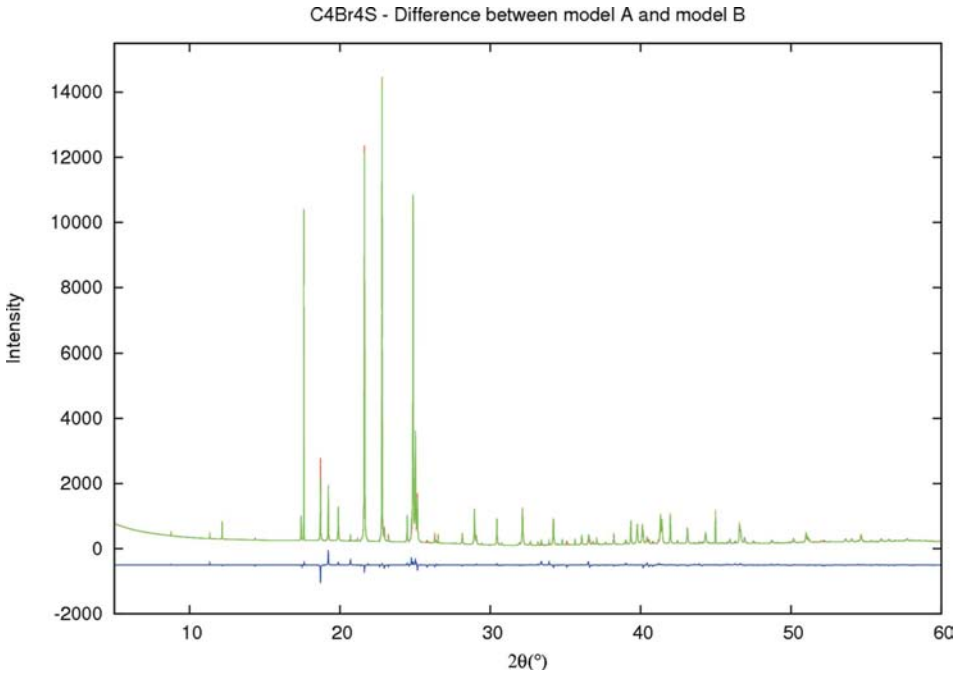

Figure 3
Calculated diffraction patterns of models A (red) and B (green) of α-C_4Br_4S (batch 1), together with their difference pattern (blue). Because of the small difference the green pattern overlaps nearly completely the red one.

3.3. Comparison between α-C_4Br_4S and β-C_4Br_4S

In both the orthorhombic α-C_4Br_4S models A (Fig. 6*c*) and B (Fig. 6*d*), and in β-C_4Br_4S (Figs. 6*a* and *b*) the positions of the Br atoms are nearly identical. The intermolecular interactions owing to bromine substitution are very close to the sums of the van der Waals radii, and do not resemble any of the known types of Br···Br interactions (Ramasubbu *et al.*, 1986). Thus, the particular packing for this tetrabromoaromatic compound is rather a consequence of the shape of the molecule. The planarity of the C_4Br_4S molecules results in an arrangement in which the Br atoms of one molecule are located in the cavities created between the Br atoms in the 2,5- and 3,4-positions of the molecule next to them. Additionally, with the thiophene molecules arranged head-to-tail, the S atom of a molecule fits between the Br atoms in the 3,4-positions of the two molecules in front of it. As a result, an efficient pseudo-hexagonal stacking arises in which the thiophene ring takes the place of a single Br atom, albeit a very large one (Fig. 7). In principle, two possible ways exist to build a structure with translational symmetry in this way: one in which the thiophene rings of neighbouring stacks are parallel, and one in which they are rotated by approximately 60°. The parallel arrangement (Fig. 8*a*) is apparently not stable, as all the observed solid-state structures of C_4Br_4S have the arrangement with the thiophene rings at an angle (Fig. 8*b*).

By combining the stacks from Fig. 8(*b*) in the head-to-tail direction, a layer is formed (Fig. 8*c*). A view perpendicular to the thiophene rings (see top section of Fig. 6*a*) shows a series of raised ridges of Br atoms located in the 2,5-positions of the thiophene rings. These ridges are flanked by valleys due to Br

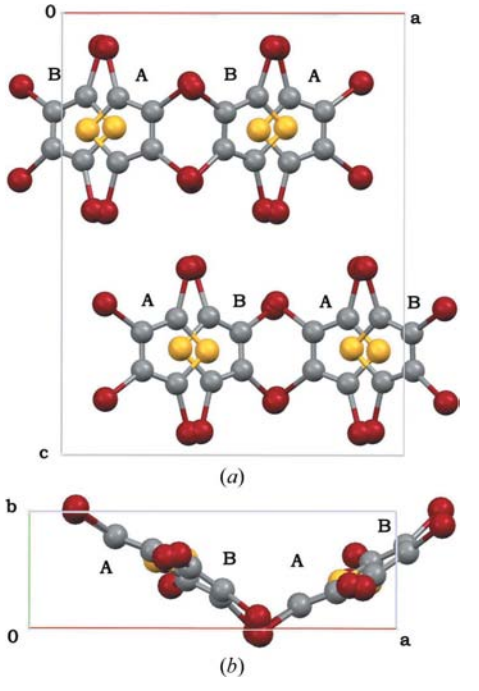

Figure 4
(*a*) Projection of both models for α-C_4Br_4S onto the *ac* plane, and (*b*) projection of both models for α-C_4Br_4S onto the *ab* plane. Br—Br distances in Å.

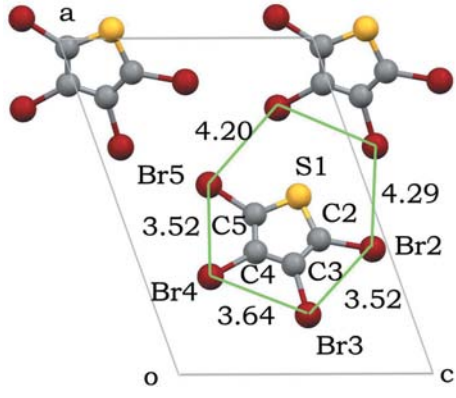

Figure 5
Projection of β-C_4Br_4S onto the *ac* plane.

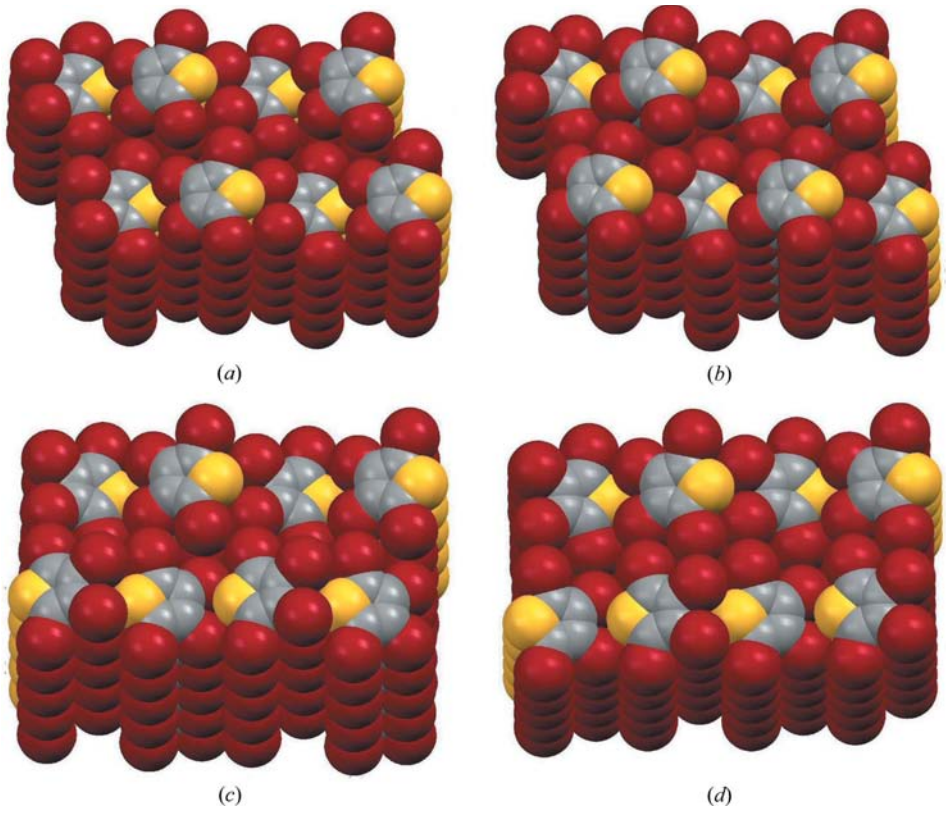

Figure 6
(*a*) First and (*b*) second possible packing for the monoclinic phase (β-C_4Br_4S), (*c*) model A and (*d*) model B for the orthorhombic phase (α-C_4Br_4S), both in the $Pca2_1$ space group.

Table 4
Results for the models A and B of α-C_4Br_4S for the neutron TOF data.

	Model A	Model B
D spacing (Å)	1.0–2.5	1.0–2.5
R_p	0.114	0.112
R_{wp}	0.125	0.121
$R(F^2)$	0.239	0.268
GOF	2.3	2.2

all S atoms of the thiophene rings point in the same direction. There are two ways of doing this, as can be seen from the relative positions of the thiophene rings pointing upwards in Figs. 6(*a*) and (*b*). When a third layer is added at the back of the first, the two structures in Figs. 6(*a*) and (*b*) are identical by rotation (by 180° along the head-to-tail axis), and thus correspond to the same single phase. The resulting structure, corresponding to β-C_4Br_4S, can be described in the space group *Pn*.

Alternatively, the S atoms of the thiophene rings in the front layer can be pointed in the opposite direction, which leads to the second set of two possible structures (Figs. 6*c* and *d*). Again, there are two ways of doing this, as can be seen from the relative positions of the thiophene rings pointing upwards in Figs. 6(*c*) and (*d*). When a third layer is then added at the back of the first, both resulting structures can be described as orthorhombic in the space group $Pca2_1$ or *Pbcm*. *Pbcm* implies mirror symmetry between the two halves of a molecule, while $Pca2_1$ implies a glide plane. The particular nature of the band splitting observed in the vibrational spectra of solid tetrabromothiophene indicates that the molecules do not have mirror symmetry, and that therefore $Pca2_1$ is the correct space group (Blockhuys *et al.*, 2000) of α-C_4Br_4S.

Several ways of switching between these three models during crystal growth are conceivable, and the high mosaicity of the orthorhombic single crystal leads us to believe that this

atoms in the 3,4-positions of the same thiophene molecule on one side, and the next thiophene molecule at the other side (note that the six mentioned Br atoms constitute the hexagons depicted in Fig. 2). An interesting feature of this arrangement is immediately clear from Fig. 6(*a*) (top section): the distances between the raised ridge and the valleys on either side of it are quite similar. This is also clear from the Br2—Br3 and Br3^{i}—Br2 distances in Figs. 2(*a*) and (*b*). Consequently, different phases can be constructed by stacking these planes on top of each other in different ways and four possibilities are given in Fig. 6.

Starting out with the layer depicted in Fig. 8(*c*), which has the thiophene rings with the S atoms oriented down and up from left to right, the first two possibilities (Figs. 6*a* and *b*) entail putting the second layer in front of the first one so that

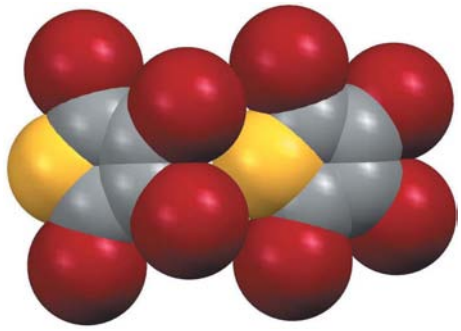

Figure 7
The pseudo-hexagonal close-packing arrangement illustrated by two adjoining molecules of tetrabromothiophene.

kind of stacking fault occurs easily. During the growth of the crystal, any of the four possibilities for growing a layer onto the previous one, presented in Fig. 6, is possible, and this will result in a change of phase if it is not a correct continuation of the mode of crystal growth. Additionally, faults can also occur during the growth of one single layer, in which the thiophene rings in the next stack are ordered parallel instead of under a 60° angle (see Fig. 8*a*), further complicating the situation.

3.4. Tetrabromoselenophene

For C_4Br_4Se only one polycrystalline phase has been found. The structure determination of C_4Br_4Se with the grid search technique and the subsequent Rietveld refinement were straightforward and resulted in an R_p of 0.058. The observed, calculated and difference patterns of the synchrotron data are given in Fig. 1(*d*), the structure in Fig. 9, and the refinement results in Table 3.

Although the Br atoms form stacks similar to those in C_4Br_4S, the Se atom is too large to fit into the cavity between the Br atoms at the 3,4-positions of the next molecule. By twisting each molecule slightly, the Br-atom packing becomes pseudo-hexagonal and the selenophene ring takes the place of one single Br atom. Fig. 9 shows that the Se atom is now located between *two* neighbouring molecules, thus requiring three different molecules for the formation of the hexagons. Another consequence of this twisting of the molecules is that the two sides of the stacks are no longer similar: one side has large ridges, and interlocks with the next stack within the same crystallographic cell, while the other side is smooth, and forms a near-perfect close-packed layer of Br atoms, which interlocks with a similar layer in a close-packing fragment along the {100} planes (see Fig. 6). It is this difference between the two sides of the stacks that resolves the packing ambiguities experienced by C_4Br_4S. While the interlocking of stacks within one unit cell leaves no opportunity for disorder to occur, *between* different unit cells the hexagonal close-packed bromine layers could give rise to disorder problems as both close-packed AB and AC layer arrangements are possible. However, since the layers are not perfectly close packed, but only nearly so, the energy difference between the two possibilities apparently is large enough to choose one arrangement unambiguously, thus leading to a single-phase structure with an *R* factor that is much lower (about 0.06) than for C_4Br_4S (about 0.10).

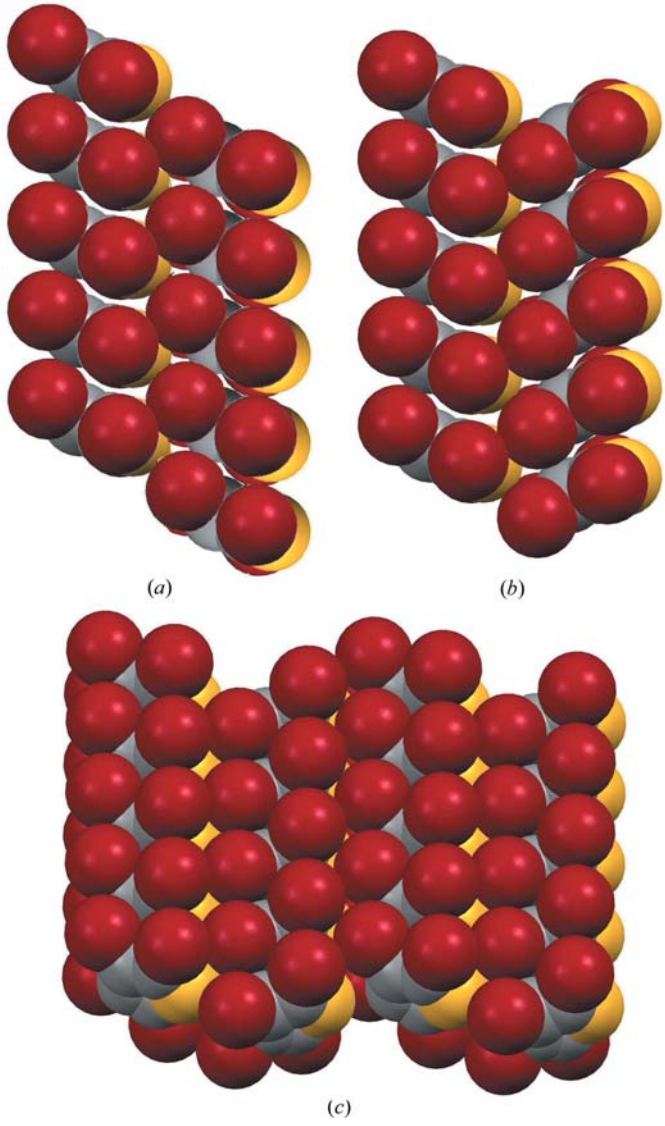

Figure 8
Two stacks can fit together with the rings (*a*) parallel and (*b*) under a 60° angle; (*c*) expansion of the stacks of (*b*) in the head-to-tail direction.

4. Conclusions

The crystal structures of C_4Br_4S and C_4Br_4Se have been presented. In the solid state C_4Br_4S displays only limited long-range order, owing to the several possibilities for the introduction of growth defects in the crystals. This is a result of the specific geometry of the C_4Br_4S ring. It appears that the orthorhombic phases are preferred when crystallization is achieved by sublimation, but that the monoclinic phase is

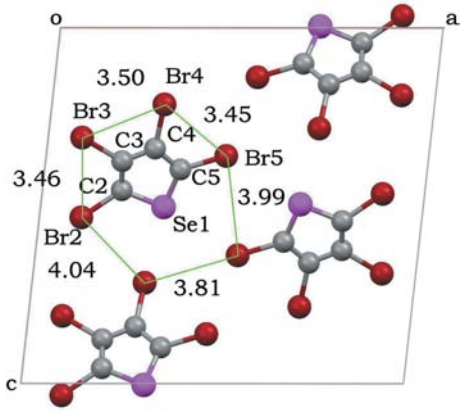

Figure 9
Projection of C_4Br_4Se onto the *ac* plane. Br—Br distances in Å.

favoured when crystallization occurs from solution. Of the two orthorhombic phases, model A appears to exhibit a slight excess in its occurrence over model B, leading us to believe that the former is the more stable form. The third phase, β-C_4Br_4S, is likewise unstable and transforms into α-C_4Br_4S over time. In C_4Br_4Se the packing ambiguities of the thiophene analogue are resolved due to the larger ring size. Yet, the packing of both compounds is based on the close packing of the Br atoms.

The authors acknowledge the ESRF (Grenoble, France) for providing the facilities to perform the synchrotron diffraction experiments, and they wish to thank W. van Beek and H. Emerich (Swiss-Norwegian beamline BM01), I. Margiolaki (ID31) and K. Goubitz (UvA) and J. B. van Mechelen (UvA) for their help in collecting the data. The authors are indebted to D. Visser of ISIS facility (UK) for the collection of the neutron powder diffraction data of α-C_4Br_4S.

References

Blockhuys, F., Rousseau, B., Peeters, L. D., Van Alsenoy, C., Geize, H. J., Kataeva, O. N., Van der Veken, B. & Herrebout, W. A. (2000). *J. Phys. Chem. A*, **104**, 8983–8988.
Chernyshev, V. V. & Schenk, H. (1998). *Z. Kristallogr.* **213**, 1–3.
Favre-Nicolin, V. & Černý, R. (2002). *J. Appl. Cryst.* **35**, 734–743.
Fitch, A. N. (1996). *Mater. Sci. Forum*, **228**, 219–222.
Fitch, A. N. (2004). *J. Res. Natl. Stand. Technol.* **109**, 133–142.
Larson, A. C. & Von Dreele, R. B. (2004). *GSAS*, Report 2004, LAUR 86–748. Los Alamos National Laboratory, New Mexico, USA.
Macrae, C. F., Edgington, P. R., McCabe, P., Pidcock, E., Shields, G. P., Taylor, R., Towler, M. & van de Streek, J. (2006). *J. Appl. Cryst.* **39**, 453–457.
Ramasubbu, N., Parthasarathy, R. & Murray-Rust, P. (1986). *J. Am. Chem. Soc.* **108**, 4308–4314.
Sas, W. H. & de Wolff, P. M. (1966). *Acta Cryst.* **21**, 826–827.
Stephens, P. W. (1999). *J. Appl. Cryst.* **32**, 281–289.
Toraya, H. (1986). *J. Appl. Cryst.* **19**, 440–447.
Visser, J. W. (1969). *J. Appl. Cryst.* **2**, 89–95.
Visser, J. W. (1986). *Powder Diffr.* **1**, 66–76.
Wolff, P. M. de (1968). *J. Appl. Cryst.* **1**, 108–113.
Zlokazov, V. B. & Chernyshev, V. V. (1992). *J. Appl. Cryst.* **25**, 447–451.